Princeton Plasma Physics Laboratory

PPPL- 4875

PPPL- 4875

STELLOPT Modeling of the 3D Diagnostic Response in ITER

S.A. Lazerson

May, 2013

Prepared for the U.S. Department of Energy under Contract DE-AC02-09CH11466.

Princeton Plasma Physics Laboratory
Report Disclaimers

Full Legal Disclaimer

Trademark Disclaimer

PPPL Report Availability

Princeton Plasma Physics Laboratory:

http://www.pppl.gov/techreports.cfm

Office of Scientific and Technical Information (OSTI):

http://www.osti.gov/bridge

Related Links:

U.S. Department of Energy

Office of Scientific and Technical Information

Fusion Links

STELLOPT Modeling of the 3D Diagnostic Response in ITER ‡

S. A. Lazerson

Princeton Plasma Physics Laboratory, Princeton, NJ

E-mail: lazerson@pppl.gov

I. T. Chapman

EURATOM/CCFE Fusion Association Culham Science Center, Abingdon, Oxfordshire, UK. OX14 3DB

Abstract. The ITER three dimensional diagnostic response to an n=3 resonant magnetic perturbation is modeled using the STELLOPT code. The in-vessel coils apply a resonant magnetic perturbation (RMP) field which generates a 4 *cm* edge displacement from axisymmetry as modeled by the VMEC 3D equilibrium code. Forward modeling of flux loop and magnetic probe response with the DIAGNO code indicates up to 20 % changes in measured plasma signals. Simulated LIDAR measurements of electron temperature indicate 2 *cm* shifts on the low field side of the plasma. This suggests that the ITER diagnostic will be able to diagnose the 3D structure of the equilibria.

PACS numbers: 52.25.Xz, 52.55.Hc, 52.65.Kj, 52.70.Ds

Keywords: Fusion, Magnetics, Diagnostics, Equilibria, Reconstruction

Submitted to: *Plasma Phys. Control. Fusion*

1. Introduction

The heat flux associated with edge localized modes (ELMs) in H-Mode plasmas requires ITER be able to suppress these phenomena. This must be done to protect the divertor components and prevent impurity influxes from this region. [1] The application of resonant magnetic perturbations (RMPs) through in-vessel coils is one such method suggested for ITER. This is a likely candidate for ELM control in ITER as various Tokamaks throughout the world have shown mitigation and suppression of ELMs through RMP application [2, 3]. However, the extent to which these 3D fields perturb the plasma boundary has varied between devices. Such variations in boundary shape can have profound implications on diagnostic interpretation and the ability to reconstruct plasma equilibria. These variations also limit the minimum plasma-wall gap at which an experiment may be run. In the MAST device, evidence of up to 5 cm variations in the plasma boundary toroidally have been documented [4]. In such cases, proper calculation of plasma stability and transport requires 3D equilibrium reconstruction.

The ability to reconstruct 3D equilibria has been developed for stellarators and has been extended to Tokamaks with applied 3D fields. The STELLOPT code [5] has been designed to fit (in a non-linear, least-squared sense) VMEC three dimensional ideal MHD equilibria [6] to various experimental diagnostic measurements around a device (in both the poloidal and toroidal directions). Originally developed to optimize stellarator equilibria for desired stability and transport properties, STELLOPT was modified to match equilibria to diagnostic measurements in the W7-AS device [7]. This work was later extended to the Large Helical Device [8], and finally to the DIII-D device [9]. The effect of discrete toroidal field coils and test blanket modules on the 3D equilibrium of ITER have been previously evaluated with VMEC [10, 11, 12]. Edge displacements were found to be less than 0.5 cm suggesting little effect on diagnostic measurements. The effect of applied RMPs on ITER equilibria have also been examined with other codes [13]. The results indicate that 'vacuum' RMP calculations, where the vacuum RMP field is added to an axisymmetric equilibrium model, are incorrect. This motivates an analysis in which the effect of such 3D fields on diagnostics measurements using a 3D equilibrium code is performed. In this paper a forward modeling of the 3D diagnostic responses of ITER is performed using the STELLOPT code. The axisymmetric and 3D equilibrium diagnostics responses of ITER are calculated in axisymmetry and for an applied RMP field. Here, the in-vessel coil system applies an $n = 3$ RMP to the plasma. Comparisons between the axisymmetric and 3D plasma diagnostic response are presented alongside a sensitivity analysis of the diagnostics measurements to equilibrium input parameters.

2. Method

The diagnostic responses of an ITER axisymmetric equilibrium and one in which the in-vessel coils apply a resonant $n = 3$ perturbation are examined through forward modeling

of diagnostics using the STELLOPT code. The STELLOPT code also evaluates a set of nearby 3D equilibria which are used to construct a Jacobian matrix of the parameter space. This provides a means to determine the sensitivity of the diagnostic responses to variations in both equilibrium profiles and the 3D geometry of applied fields.

The STELLOPT code optimizes VMEC equilibria to a given set of constraints utilizing various non-linear techniques. A general analogy can be made to non-linear curve fitting where a set of input coefficients are sought which minimize the fit to a set of data points in a least squared sense. For equilibrium reconstruction the input coefficients are the input parameters to the VMEC equilibrium. This can include the pressure profile, current profile, total enclosed toroidal flux, toroidal current, and vacuum field coil currents. The measured diagnostic signals in the experiment then become the non-linear curve to which a fit is sought. The quantitative measure of how well a given equilibrium matches experimental data is known as chi-squared $\chi^2 = \sum \left(x_{data} - x_{sim}\right)^2 / \sigma^2$, where σ can be taken to be the error bar in a measured quantity and the sum is over all experimental measurements. In practice, each experimentally measured datapoint (eg. Te, flux, Ti) has a unique error bar (σ) in STELLOPT, however in some cases larger σ values are utilized to avoid pathalogical equilibria which satisfy the properties of a local-minima. Various methods of achieving this optimization have been implemented in STELLOPT, but for the work presented here the Levenberg-Mardquardt method is utilized [14]. This is advantageous, as this method calculates a parameter space Jacobian which provides information about the sensitivity of diagnostic measurements to variations in plasma parameters. As the ITER experiment has not yet begun operation, we can only provide a forward modeling of the diagnostic response. Equilibria are calculated and then the diagnostic response of those equilibria are compared. In a full reconstruction, an approximate parameter space Hessian is calculated which is used to provide confidence intervals for the reconstructed parameters. Such confidence intervals

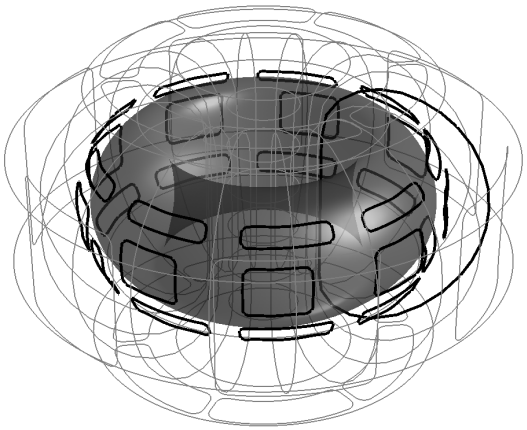

Figure 1. ITER coil set utilized for free boundary VMEC equilibria. The in vessel coils and one toroidal field coil have been highlighted for clarity. The axisymmetric VMEC equilibrium is also plotted for reference.

indicate which diagnostics provide unique constraints on the reconstruction. For example, a point measurement of the electron temperature provides a tight constraint on the magnitude of the profile and the location of a flux surface. In contrast, the flux loop signals contains a convolution of plasma pressure profile, current profile and shape information for the general 3D problem. The goal of reconstruction is to deconvolve signals and provide an accurate representation of the equilibrium subject to the constraints of the equilibrium model.

The VMEC code is utilized to calculate ideal 3D MHD equilibria for this work. In this code, an ideal MHD energy functional of the form

$$W = \int \left(\frac{B^2}{2\mu_0} + \frac{p}{\gamma - 1} \right) dV \tag{1}$$

is minimized subject to the constraint of a global magnetic topology, namely that a continuous set of nested flux surfaces exists everywhere in the domain of the equilibria (equivalent to $\vec{B} \cdot \nabla \psi = 0$). Here B is the magnetic field intensity, μ_0 is the permeability of free space, p is the total plasma pressure, γ is the adiabatic index, and the volume integral is over the domain of the plasma. The domain of the code is defined by a plasma edge, in our case where the electron temperature approaches zero, and an inverse Fourier representation is utilized in the poloidal and toroidal directions ($m = [0, 12], n = [-9, 9]$). Equilibria are considered converged for 99 radial surfaces at a force balance criterion of $FTOL = 1.0 \times 10^{-12}$. The free boundary approach to the code requires the fields of the ITER coilset to be mapped to a cylindrical grid and the normal component of the field on the equilibrium boundary minimized. The full coil-set utilized in these calculations can be seen in Figure 1. The coil field is passed to VMEC on a cylindrical grid (the 'mgrid' file generated by the MAKEGRID code). The grid is defined by $R = [3.5, 9.5]\ m$, $Z = [-5.5, 5.5]\ m$, and $\phi = [0, 2\pi]\ rad$, with $nr = 121$, $nz = 221$, and $nphi = 72$ grid points.

The VMEC equilibrium is defined by a set of input parameters: the enclosed toroidal flux (PHIEDGE), net toroidal current (CURTOR), vacuum field currents (EXTCUR), pressure profile (AM), current profile (AC), and pressure scaling factor (PRES_SCALE). The profile functions are parameterized as functions of the normalized toroidal flux. Experimentally the total plasma pressure profile is not measured, but rather various species densities and temperatures are measured. To this end the STELLOPT code parameterizes the electron temperature (T_e), electron density (n_e), and ion temperature (T_i), then constructs the pressure profile from these quantities. The inclusion of the pressure scaling factor (P_{fact}) in the optimization allows measurements of stored energy to be matched (flux loops and diamagnetic loops), independent of profile variations.

$$p(s) = P_{fact} n_e(s) [T_e(s) + T_i(s)] \tag{2}$$

Here, s is normalized toroidal flux. It is the goal of the reconstruction to find the values of these input equilibrium parameters which best fit diagnostic measurements in an experiment.

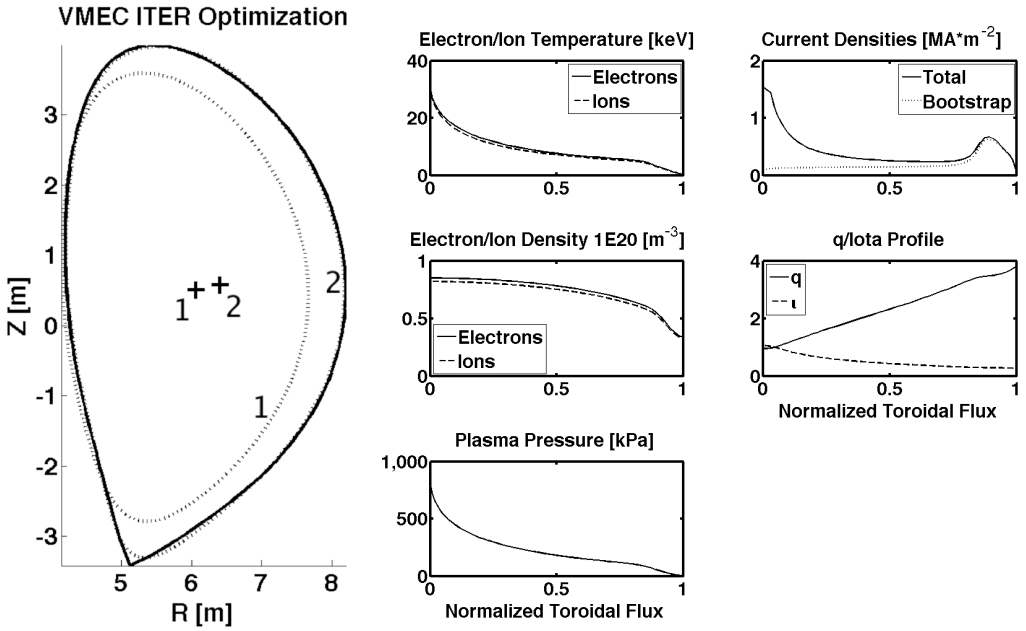

Figure 2. ITER boundary optimization and profiles utilized for forward modeling. The ITER coil currents were optmized in axisymmetry to provide a best fit between the VMEC equilibria and the ITER target separatrix (solid line). Initial (1) and final (2) VMEC boundaries (dashed line) and magnetic axes (+) are plotted. Profiles determined by CORSICA are utilized in the VMEC equilibrium calculations. The extrapolated plasma pressure profile is obtained from the various species profiles.

In order to forward model diagnostic responses, profiles are first obtained from the CORSICA code [15]. This is done as experimental data from ITER does not yet exist. Figure 2 depicts the kinetic profiles, current density, and the VMEC optimized equilibrium boundary. The STELLOPT code was the utilized to optimize the free boundary axisymmetric solution to the ITER target separatrix through variation of the axisymmetric coil currents. Here the chi-squared for the fit to the target separatrix was decreased from 3.0926×10^7 to 2.3008×10^5. In this configuration RBtor is 32.86 $T-m$, the total enclosed toroidal flux is found to be 120.6 Wb, with $q0 = 0.58$, $q95 = 3.1$, and $I_{tor} = 15\ MA$. This value of $q0$ is low, as the expected value should be $q0 \geq 0.9$, but should pose no issue on the boundary calculation. The initial and final VMEC axis and boundary plotted against the target ITER separatrix showing good agreement between both. Only axisymmetric coil currents were optimized and no non-axisymmetric coils were energized. This provides a baseline axisymmetric equilibrium configuration to which non-axisymmetric RMP fields may be applied. The non-axisymmetric field considered here has an $n = 3$ feature and utilizes the in-vessel coil currents to excite such a field (in upper coils in [A]: 23220. -86940. 63630. 23310. -86940. 63630. 23310. -86940. 63630; in mid-plane coils: 0. 77940. -77940. 0. 77940. -77940. 0. 77940. -77940; in lower coils: -27810. -60210. 88020. -27810. -60210. 88020. -27810. -60210.

88020)[13]. These coil current approach the maximum rated coil current (90000 [A]), placing an upper limit on the diagnostic response and edge displacement. It should be noted that ELM suppression may be possible at lower coil currents [16].

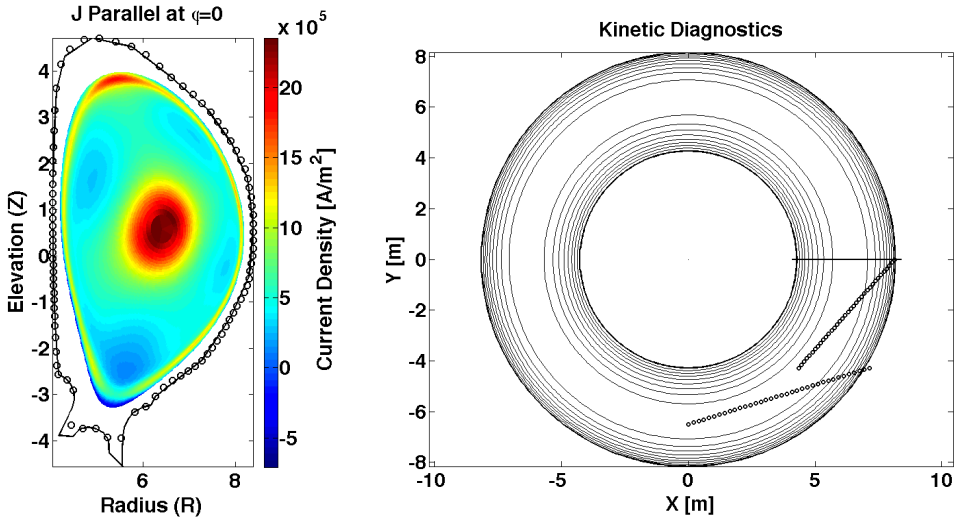

Figure 3. Locations of forward modeled diagnostics. Axisymmetric ITER parallel current density is depticted with the ITER first wall and poloidal locations of the 89 simulated flux loops (left). Profile diagnostics for LIDAR (solid line) and charge exchange recombination (circles) are depicted against the axisymmetric flux surfaces in the $z = 0$ plane (left).

The STELLOPT code has modules which calculate synthetic diagnostics for magnetics, electron temperature, electron density, line integrated electron density, ion temperature, and motional Stark effect (MSE) diagnostics allowing these measurements to be fited during reconstruction. As the details of these systems on ITER (at the time of this work) were still under development, a set of trial diagnostic geometries were assumed (Figure 3). A set of 89 toroidally symmetric flux loops equidistant in poloidal angle were placed along the first wall. A grid of 89 points poloidaly and 89 points toroidally (equally spaced) was placed on the first wall and the components of the magnetic field measured (not shown). In both cases, only the field due to the plasma was calculated utilizing a virtual casing principle [17] and integration along magnetic diagnostics was preformed using the DIAGNO code [18, 19]. It should be noted that in a fully superconducting steady-state machine, magnetic diagnostics only sense the plasma response and any changes in the coil currents. They do not measure the vacuum field since diagnostic integration usually begins after the toroidal and poloidal fields are ramped. It should also be noted that in the real device the closest the diagnostics may be placed is on the inner side of the vessel wall, $\sim 0.5\ m$ away from the plasma. Thus these simulations are an attempt to place an upper bound on the magnetic diagnostic response. The LIDAR system was assumed to be located at $z = 0.0$ measuring radially inward from the $phi = 0$ plane from $R = 4.1$ to $R = 8.4\ m$ with a resolution of $1.7\ cm$. Ion temperatures were measured along two beam lines with 36 points along each line.

These diagnostic serve only to help better understand the role 3D equilibria may play in the fit to experimental data in ITER. Simulation of an MSE diagnostic is neglected in this work due to the complex dependence of beam and viewing geometry on diagnostic signal. Line integrated electron densities were neglected as well.

While a meaningful reconstruction is not possible before operation of the device, STELLOPT can calculate the parameters space Jacobian around a given equilibria, providing a measure of the sensitivity of each diagnostic measure to each parameter variation. This is achieved by perturbing each equilibria input parameter by 1%, recalculating the equilibria, and the resultant diagnostic response. The parallelization of this step in STELLOPT and capability of VMEC to use the previous equilibria as an initial guess for the new equilibrium make this step particularly efficient. Assuming that there are at least as many processors as variables to vary the total calculation time for such a Jacobian evaluation is typically less than the time it would take to evaluate two successive equilibrium.

3. Results

Calculations of the ITER equilibrium were performed for axisymmetric and non-axisymmetric configurations (n=3 in-vessel coil configuration) using the VMEC code. The maximum DC coil current utilized was $\sim 88\ kA-t$, which is nearing the maximum coil current of 90 $kA-t$. Comparison between the configurations indicated up to $\pm 4\ cm$ deviations from axisymmetry (Figure 4). These deviations peaked toward the top and bottom of the equilibrium. The high-field side indicated a displacement but local deviations in this region were small. The low-field side of the plasma indicated greater local deviations in displacement. Such displacements are consistent with similar calculations done for DIII-D using the VMEC code. This is within the predicted limits of the ITER control system ability to confine the plasma. It is important to note that all profiles were assumed fixed with respect to toroidal flux. As a result, they do not account for the 'density pumpout' associated with RMP application in DIII-D for ITER-similar plasmas.

The diagnostic response of the flux loops and magnetic field probes suggest that outboard side of the plasma has the greatest sensitivity to 3D variations. Figure 5 indicates deviations from axisymmetric values of up to 20% on the low field side of the plasma. These variations are greatest approximately half way up the inner wall. It should be noted that a large current density is present near the top of the equilibrium in Figure 3. This current density has a helical feature in the non-axisymmetric equilibria, which accounts for the change in flux loop signals. Variations on the lower half of the device were also large at around 10%. The high-field side of the device indicated only small changes in the plasma response. The magnetic probes indicate a torodial and poloidal sensitivity to the various field components. The radial and vertical field saw up to 20 G deviations in field strength when compared to axisymmetry. These signals are small compared to the axisymmetric field $\sim$ 1%. The toroidal field saw

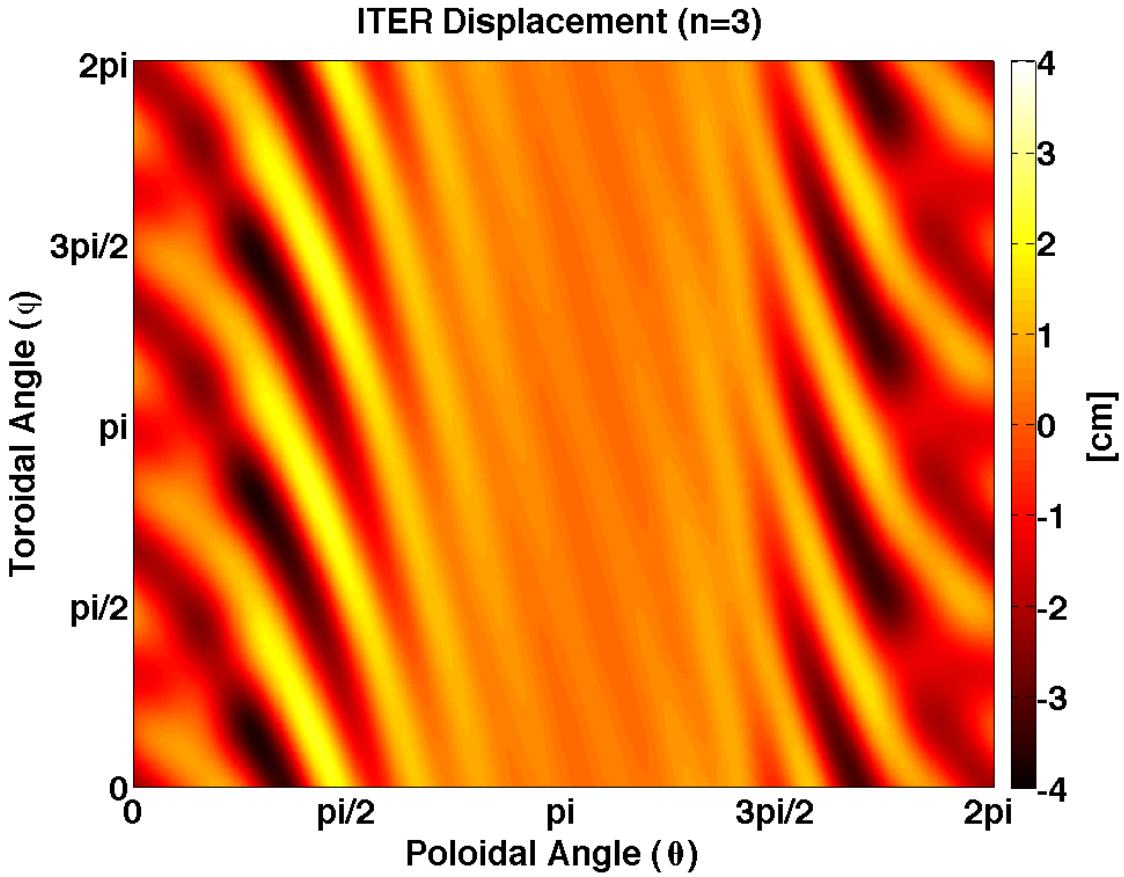

Figure 4. Radial displacement in ITER due to applied $n = 3$ resonant field. The regions around the low-field side ($\theta = 0$ and $\theta = 2\pi$) indicate the largest displacement ($\sim$ 8 *cm* peak-to-peak) relative to axisymmetry while the high-field side ($\theta = \pi$) indicates a small rigid shift with minimal poloidal or toroidal variation in this region.

a similar plasma response but when compared to the axisymmetric signal showed a greater overall sensitivity ($\sim$ 50% variations in field strength). An array of B-Field probes on the outboard mid-plane should be able to distinguish modes through toroidal field measurements.

Forward modeling of the LIDAR diagnostic signals suggests that various non-axisymmetric boundary effects could be distinguished. The LIDAR scattering system detects $\sim$ 2 *cm* of motion in the plasma edge due to 3D effects. This is greater than the resolution of the desired parameters for the ITER LIDAR system suggesting that in the real device such an effect can be measured. The high field side also experiences small deviations but those may well be below the experimental noise in the signal. This suggests that during RMP experiments in ITER, 2D equilibrium fitting should neglect the outboard LIDAR data points in order to provide a more consistent fit. Additionally, diagnosis of the 3D structure of the plasma could benefit from enhanced spatial resolution on the low-field side. It should be noted that full 3D equilibrium reconstruction is a relatively slow process compared to the real time 2D equilibrium

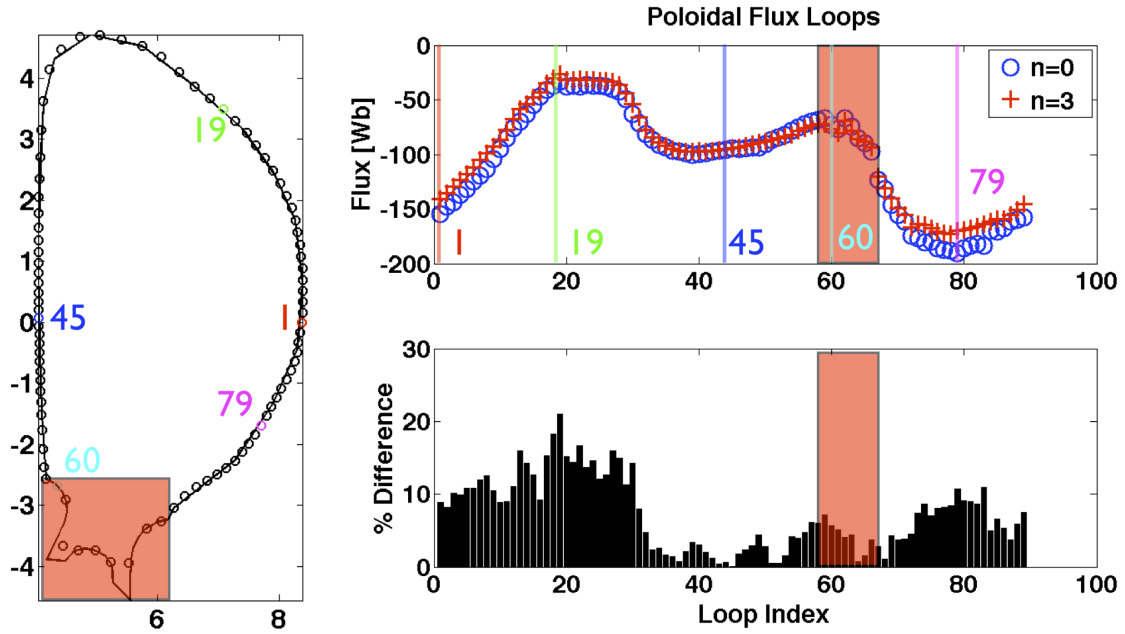

Figure 5. Poloidal flux loop response to applied resonant mangetic perturbation ($n = 3$). ITER first wall and simulated flux loops are depicted (left). Index number for select loops are shown. Flux loop response (top right) and difference from axisymmetry are plotted (bottom right). The loops on the upper outboard midplane show the greatest sensitivity this boundary perturbation. Shaded regions indicate the divertor region where it may be difficult to place probes.

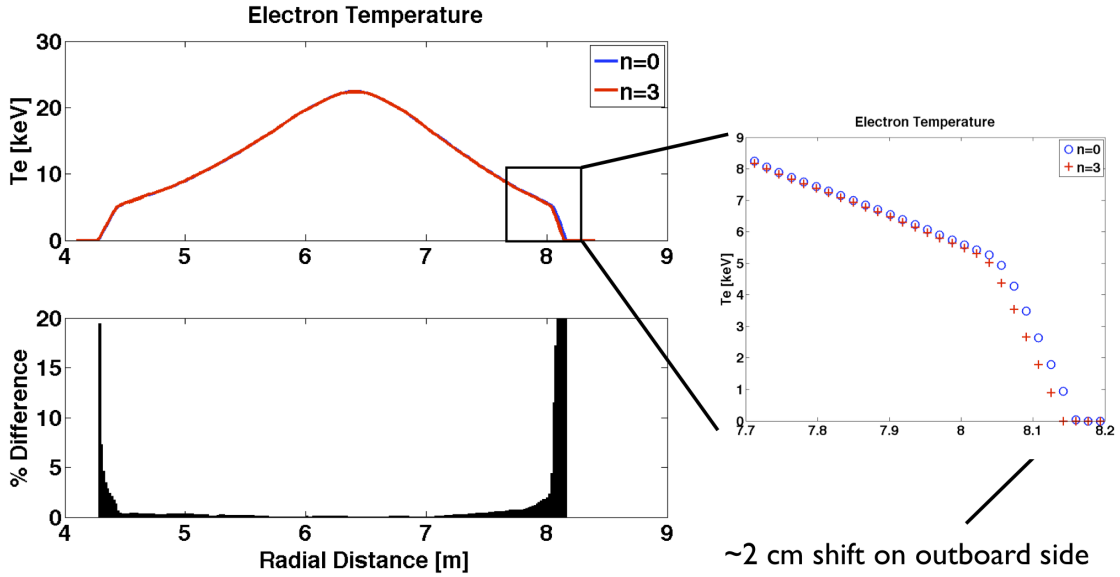

Figure 6. Simulated ITER LIDAR scattering diagnostic response. Comparrison between the axisymmetric ($n = 0$) and non-axisymmetric ($n = 3$) equilibria indicate that the sensitivity to variations in the plasma edge is greatest on the low field side of the plasma.

control available in modern Tokamaks.

The modeled response of the charge exchange system suggests little sensitivity to deviations from axisymmetry. This is attributed to poor resolution at the edge for the modeled system. In general, beam-line measurements result in an increased radial resolution toward the magnetic axis and decreased resolution toward the plasma edge. Enhanced edge resolution should produce a similar sensitivity as was indicated by forward modeling of the LIDAR system.

The parameter space Jacobian calculated by STELLOPT provides information regarding the variation of diagnostic signals with respect to various parameters. In general, there is a strong sensitivity in nearly all signals to variations in the pressure profile. This is attributed to strong pressure driven currents at finite beta ($\sim 2\%$) in an H-mode plasma. Variations in the current profile were on the order of those attributed to variations in the plasma boundary (external currents). It is likely that only a few moments of a generalized current profile will be discernible in the real experiment. This highlights the need of reconstruction to de-convolve the various magnetic signals at various toroidal locations.

4. Discussion

The ability to reconstruct 3D equilibria from diagnostic measurements can now regularly be done for both fully 3D systems (stellarators) and those with a high degree of axisymmetry (Tokamaks). Forward modeling of the 3D diagnostic response in ITER has been preformed with the STELLOPT code for the first time. The diagnostic response of simulated flux loops, magnetic field probes, LIDAR, and charge exchange recombination spectroscopy have been investiaged both in axisymmetry and for an applied RMP ($n = 3$) in ITER. The applications of RMP's result in an 8 cm peak-to-peak variation in the plasma boundary. Flux loops suggest the greatest sensitivity to non-axisymmetric fields will be found on the low field side of the plasma above the midplane. This is attributed to a large edge parallel current in this region becoming distorted in the VMEC equilibrium. Magnetic probe data suggests a similar behavior for identification of toroidal equilibrium mode structure. Simulation of LIDAR data suggests a sensitivity to boundary perturbations on the low-field side of the plasma as well. The simulated charge-exchange data did not possess enough radial resolution toward the plasma edge to discriminate the effect of applying an RMP. This could be easily alleviated by dedicating a second camera system to look in higher resolution toward the plasma edge. The MSE system was neglected in these calculations as difficulties separating viewing geometry issues from 3D effects complicate such an analysis. Such work is left to the future when diagnostic geometries have been more accurately defined.

One interesting feature to note is the low sensitivity to RMP application on the high field side suggested by the VMEC equilibria. The motion of the high-field plasma boundary could be considered a small rigid shift in the plasma. It is possible that as RMP fields are rotated in ITER the plasma control system (PCS) could interpret

such shifts as a growing n=0 mode. This would suggest that when fitting axisymmetric equilibria to diagnostic measurements, emphasis should be placed on fitting the high-field plasma measurements. The average of two loops, one on high field side and one on the low field side, at different toroidal sectors may also help stabilize the 2D plasma control system to 3D perturbations. Whenever possible, the full 3D plasma response should be calculated when fitting equilibria to experimental measurements for data analysis. This will guarantee model consistency with respect to geometry even if a given equilibrium model lacks other effects (flow, shielding, etc).

Acknowledgments

The author would thank W. Cooper, S. Hudson, D. Gates, and M. Zarnstorff for their valuable discussions on equilibrium and ITER. The author would also like to thank S. Hirshman for access to the VMEC code. The author would also like to thank Y. Gribov for access to the CORSICA data simulations and commentary on ITER.

[1] R.J. Hawryluk, D.J. Campbell, G. Janeschitz, P.R. Thomas, R. Albanese, R. Ambrosino, C. Bachmann, L. Baylor, M. Becoulet, I. Benfatto, J. Bialek, A. Boozer, A. Brooks, R. Budny, T. Casper, M. Cavinato, J.-J. Cordier, V. Chuyanov, E. Doyle, T. Evans, G. Federici, M. Fenstermacher, H. Fujieda, K. G'al, A. Garofalo, L. Garzotti, D. Gates, Y. Gribov, P. Heitzenroeder, T.C. Hender, N. Holtkamp, D. Humphreys, I. Hutchinson, K. Ioki, J. Johner, G. Johnson, Y. Kamada, A. Kavin, C. Kessel, R. Khayrutdinov, G. Kramer, A. Kukushkin, K. Lackner, I. Landman, P. Lang, Y. Liang, J. Linke, B. Lipschultz, A. Loarte, G.D. Loesser, C. Lowry, T. Luce, V. Lukash, S. Maruyama, M. Mattei, J. Menard, M. Merola, A. Mineev, N. Mitchell, E. Nardon, R. Nazikian, B. Nelson, C. Neumeyer, J.-K. Park, R. Pearce, R.A. Pitts, A. Polevoi, A. Portone, M. Okabayashi, P.H. Rebut, V. Riccardo, J. Roth, S. Sabbagh, G. Saibene, G. Sannazzaro, M. Schaffer, M. Shimada, A. Sen, A. Sips, C.H. Skinner, P. Snyder, R. Stambaugh, E. Strait, M. Sugihara, E. Tsitrone, J. Urano, M. Valovic, M. Wade, J. Wesley, R. White, D.G. Whyte, S. Wu, M. Wykes, and L. Zakharov. Principal physics developments evaluated in the iter design review. *Nuclear Fusion*, 49(6):065012, 2009.

[2] T. E. Evans, R. A. Moyer, P. R. Thomas, J. G. Watkins, T. H. Osborne, J. A. Boedo, E. J. Doyle, M. E. Fenstermacher, K. H. Finken, R. J. Groebner, M. Groth, J. H. Harris, R. J. La Haye, C. J. Lasnier, S. Masuzaki, N. Ohyabu, D. G. Pretty, T. L. Rhodes, H. Reimerdes, D. L. Rudakov, M. J. Schaffer, G. Wang, and L. Zeng. Suppression of Large Edge-Localized Modes in High-Confinement DIII-D Plasmas with a Stochastic Magnetic Boundary. *Phys. Rev. Lett.*, 92(23):235003–+, 2004.

[3] K. H. Burrell, T. E. Evans, E. J. Doyle, M. E. Fenstermacher, R. J. Groebner, A. W. Leonard, R. A. Moyer, T. H. Osborne, M. J. Schaffer, P. B. Snyder, P. R. Thomas, W. P. West, J. A. Boedo, A. M. Garofalo, P. Gohil, G. L. Jackson, R. J. La Haye, C. J. Lasnier, H. Reimerdes, T. L. Rhodes, J. T. Scoville, W. M. Solomon, D. M. Thomas, G. Wang, J. G. Watkins, and L. Zeng. ELM suppression in low edge collisionality H-mode discharges using n = 3 magnetic perturbations. *Plasma Physics and Controlled Fusion*, 47:B37–B52, 2005.

[4] I T Chapman, W A Cooper, A Kirk, C J Ham, J R Harrison, A Patel, S D Pinches, R Scannell, A J Thornton, and the MAST Team. Three-dimensional corrugation of the plasma edge when magnetic perturbations are applied for edge-localized mode control in mast. *Plasma Physics and Controlled Fusion*, 54(10):105013, 2012.

[5] D.A. Spong, S.P Hirshman, L.A. Berry, J.F. Lyon, R.H. Fowler, D.J. Strickler, M.J. Cole, B.N. Nelson, D.E. Williamson, A.S. Ware, D. Alban, R. Sànchez, G.Y. Fu, D.A. Monticello, W.H.

Miner, and P.M. Valanju. Physics issues of compact drift optimized stellarators. *Nucl. Fusion*, 41:711–716, 2001.

[6] S. P. Hirshman and J. C. Whitson. Steepest-descent moment method for three-dimensional magnetohydrodynamic equilibria. *Phys. Fluids*, 26(12):3553–3568, 1983.

[7] M.C. Zarnstorff, A. Weller, J. Geiger, E. Fredrickson, S. Hudson, J.P. Knauer, A. Reiman, A. Dinklage, G.Y. Fu, L.P. Ku, D. Monticello, A. Werner, the W7-AS Team, and the NBI-Group. Equilibrium and Stability of High-Beta Plasmas in Wendelstein 7-AS. *Fusion Sci. and Tech.*, 46, 2004.

[8] S. Lazerson, D. Gates, D. Monticello, D. Neilson, N. Pomphrey, A. Reiman, S. Sakakibara, and S. Suzuki. Equilibrium reconstruciton on the large helical device. In *38th EPS Conference on Plasma Physics*, page O5.417, 2011.

[9] S. Lazerson, E. Lazarus, S. Hudson, N. Pablant, and D. Gates. 3d equilibrium effects due to rmp application on diii-d. In *39th EPS Conference and 16th Int. Congress on Plasma Physics*, page P4.077, 2012.

[10] E. Strumberger, S. Gunter, P. Merkel, E. Schwarz, and C. Tichmann. Self-consistent three-dimensional computations of non-axisymmetric iter equilibria. *Nuclear Fusion*, 50(2):025008, 2010.

[11] K. Shinohara, T. Kurki-Suonio, D. Spong, O. Asunta, K. Tani, E. Strumberger, S. Briguglio, T. Koskela, G. Vlad, S. Gunter, G. Kramer, S. Putvinski, K. Hamamatsu, and ITPA Topical Group on Energetic Particles. Effects of complex symmetry-breakings on alpha particle power loads on first wall structures and equilibrium in iter. *Nuclear Fusion*, 51(6):063028, 2011.

[12] D. A. Spong. Three-dimensional effects on energetic particle confinement and stability. *Physics of Plasmas*, 18(5):056109, 2011.

[13] M. Becoulet, F. Orain, P. Maget, N. Mellet, X. Garbet, E. Nardon, G.T.A. Huysmans, T. Casper, A. Loarte, P. Cahyna, A. Smolyakov, F.L. Waelbroeck, M. Schaffer, T. Evans, Y. Liang, O. Schmitz, M. Beurskens, V. Rozhansky, and E. Kaveeva. Screening of resonant magnetic perturbations by flows in tokamaks. *Nuclear Fusion*, 52(5):054003, 2012.

[14] D. W. Marquardt. An algorithm for least-squares estimation of nonlinear parameters. *SIAM*, 11, 1963.

[15] J. A. Crotinger, L. LoDestro, L. D. Pearlstein, A. Tarditi, T. A. Casper, and E. B. Hooper. Corsica: A comprehensive simulation of toroidal magnetic-fusion devices. Technical Report UCRL-ID-126284, Lawrence Livermore National Laboratory, Apr 1997.

[16] T.E. Evans, D.M. Orlov, A. Wingen, W. Wu, A. Loarte, T.A. Casper, O. Schmitz, G. Saibene, and M.J. Schaffer. 3d vacuum magnetic field modeling of the iter elm control coils during standard operating scenarios. In *Real Time Conference, 1999. Santa Fe 1999. 11th IEEE NPSS*, pages 388 –391, 2012.

[17] S A Lazerson. The virtual-casing principle for 3d toroidal systems. *Plasma Physics and Controlled Fusion*, 54(12):122002, 2012.

[18] H.J. Gardner. Diagnostic coils on the w vii-as stellarator using a three-dimensional equilibrium code. *Nucl. Fusion*, 30(8):1417–1424, 1990.

[19] S A Lazerson, S Sakakibara, and Y Suzuki. A magnetic diagnostic code for 3d fusion equilibria. *Plasma Physics and Controlled Fusion*, 55(2):025014, 2013.

The Princeton Plasma Physics Laboratory is operated
by Princeton University under contract
with the U.S. Department of Energy.

Information Services
Princeton Plasma Physics Laboratory
P.O. Box 451
Princeton, NJ 08543

Phone: 609-243-2245
Fax: 609-243-2751
e-mail: pppl_info@pppl.gov
Internet Address: http://www.pppl.gov